Article:
Mirsaneh, M., Reaney, I.M., Hatton, P.V. et al. (2004) Characterization of high-fracture toughness K-fluorrichterite-fluorapatite glass ceramics. Journal of the American Ceramic Society, 87 (2). pp. 240-246. ISSN: 0002-7820

https://doi.org/10.1111/j.1551-2916.2004.00240.x

journal

J. Am. Ceram. Soc., 87 [2] 240–46 (2004)

Characterization of High-Fracture Toughness K-Fluorrichterite-Fluorapatite Glass Ceramics

Mehdi Mirsaneh,[†] Ian M. Reaney,[*,†] Paul V. Hatton,[‡] and Peter F. James[*,†]

Department of Engineering Materials, The University of Sheffield, Sheffield S1 3JD, United Kingdom

Center for Biomaterials and Tissue Engineering, School of Clinical Dentistry, The University of Sheffield, Sheffield S10 2TA, United Kingdom

Stoichiometric K-fluorrichterite (Glass A) and the same composition with 2 mol% P_2O_5 added (Glass B) were prepared and then heat-treated isothermally from 550°–1000°C with 50°C intervals. Samples were characterized using X-ray diffraction (XRD) and transmission electron microscopy (TEM). The biaxial flexural strength and indentation fracture toughness of heat-treated glass specimens were also determined for both materials. XRD traces and TEM images showed similar phase evolution and fine microstructures for both systems at ≤950°C, with mica and diopside reacting with residual glass to form K-fluorrichterite as the temperature was increased from 650°C. However, in Glass B, fluorapatite was also present at >800°C. In contrast, coarser microstructures were observed at 1000°C, with larger K-fluorrichterite (20 μm) and enstatite (10 μm) crystals in Glasses A and B, respectively. The highest fracture toughness (2.69 ± 0.01 MPa·m$^{1/2}$) and biaxial strength (242.6 ± 3.6 MPa) were recorded for Glass B heat-treated at 1000°C. This was attributed to the presence of enstatite coupled with an interlocked lath-like crystalline microstructure.

I. Introduction

Generally, bioactive materials for bone-tissue repair are divided into two categories: osteoconductive and osteoinductive. Osteoconductive biomaterials encourage the formation of new bone tissue on their surface after implantation into existing bone. Osteoinductive biomaterials are able to induce *de novo* formation of bone tissue, irrespective of the site of implantation. Biomaterials that contain apatite are usually osteoconductive, because apatite provides a biocompatible interface along which bone migrates.[1,2] Hench[1,3] suggested that specific glass and glass-ceramic compositions were able to bond to living tissue and elicit both intracellular and extracellular responses, resulting in so-called osteoproductivity. However, the mechanical properties of these bioactive materials are often poor. Significant effort has therefore been directed at the development of bioactive glass ceramics with high strength.[4–6] The high strength and fracture toughness apatite-wollastonite (A/W) glass ceramic (with bending strength of 215 MPa and fracture toughness of 2.0 MPa·m$^{1/2}$)[7] has been used successfully in a number of applications in medicine.[8] However, surface crystallization of this glass ceramic system makes it difficult to manufacture complex or custom prostheses via a conventional melting and casting route. Powder processing must be used, with associated limitations.

High strength and toughness chain silicate glass ceramics, including canasite, K-fluorrichterite, and enstatite, have very good mechanical properties because of an interlocking acicular microstructure.[9] These glass ceramics can be cast to shape using conventional techniques, heat-treated to a final glass-ceramics product and exhibit volume crystallization. However, these materials are not considered to be bioactive.[10] There have been recent attempts to improve the osteoconductive potential of canasite glass ceramics by introduction of phosphate to induce crystallization of an apatite phase.[2] Promising *in vitro* data has been reported for these modified canasite glass ceramics, but this is yet to be confirmed *in vivo*.[11] Although progress with canasite systems is encouraging, there have been no reports to date of similar modifications to high-strength K-fluorrichterite to improve biocompatibility.

K-fluorrichterite ($KNaCaMg_5Si_8O_{22}F_2$) is a member of amphibole chain silicate group, which has been assigned a space group of I2/m.[12] The general formula for amphibole crystals has been defined[13] as: $A_{0-1}B_2C_5T_8O_{22}(OH,F)_2$, where A = Na, K; B = Na, Li, Ca, Mn, Fe^{2+}, Mg; C = Mg, Fe^{2+}, Mn, Al, Fe^{3+}, Ti; T = Si, Al, and therefore richterite is considered as a sodic-potassic amphibole with a formula: $KNaCaMg_5Si_8O_{22}(OH)_2$. In the case of potassium fluorrichterite, the formula is $KNaCaMg_5Si_8O_{22}F_2$, wherein OH^- and Na^+ are replaced by F^- and K^+, respectively.[9,14] The crystal chemistry of K-fluorrichterite has been described in detail.[12,15] Grossman[16] demonstrated that glasses based on fluoroamphiboles with different compositions, including fluorrichterite, fluormagnesiorichterite, and protoamphiboles, may undergo crystallization and Beall *et al.*[14,17] examined the methods of improving their properties.

Phase evolution in this system was first investigated by Beall,[9] then confirmed by Omar *et al.*[18] and discussed in detail by Mirsaneh *et al.*[19] They suggested phase separation initially occurs in which one phase is close in composition to tetrasilisic fluormica, $(K,Na)Mg_{2.5}Si_4O_{10}F_2$, which then crystallized at ~650°C. At higher temperatures (700°C), diopside ($CaMgSi_2O_6$) forms, which reacts with mica and residual glass to form K-fluorrichterite at 750°C. El-Shennawi *et al.*[20] investigated the effect of fluorine and phosphate on this system using XRD and reported that P_2O_5 encourages the crystallization of enstatite at 1000°C. The effects of magnesium and sodium content on the microstructure of these glass ceramics were also investigated by Denry and Holloway.[21,22] Although the microstructure of modified compositions of K-fluorrichterite glass ceramics[9,21,22] consist of large acicular crystals (20 μm), stoichiometric compositions have a very fine microstructure (0.2 μm).[19]

As outlined above, there is the possibility of producing a modified K-fluorrichterite glass ceramic with osteoconductive potential. This paper describes the addition of P_2O_5 to the stoichiometric K-fluorrichterite composition to crystallize a low-volume fraction of an apatite phase. The effect of this addition on phase evolution, indentation fracture toughness, and biaxial flexure strength is reported.

N. Padture—contributing editor

Manuscript No. 10311. Received June 12, 2003; approved August 24, 2003.

Funding provided by the Ministry of Science, Research and Technology (MSRT), Iran.

*Member, American Ceramic Society.

†Department of Engineering Materials.

‡Center for Biomaterials and Tissue Engineering.

Table I. Chemical Composition of Glasses in Mol%

	Reagent-Grade Chemicals					
	SiO_2	Na_2O	K_2O	MgO	CaF_2	P_2O_5
Glass A	53.37	3.33	3.33	33.35	6.62	0
Glass B	52.26	3.26	3.26	32.66	6.56	2

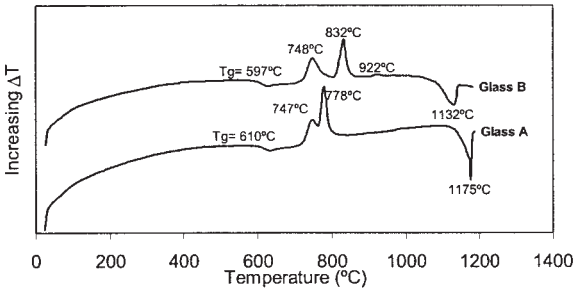

Fig. 1. DTA traces of Glass A and Glass B.

II. Experimental Procedures

(1) Glass Preparation and Heat Treatments

Two compositions, stoichiometric ($KNaCaMg_5Si_8O_{22}F_2$) (Glass A) and stoichiometric with 2 mol% P_2O_5 (Glass B) (Table I), were prepared using reagent-grade chemicals, except SiO_2, which was used as silica sand (type L30A 99.8% SiO_2, Loch Aline crystal glass sand, Tilcon (South) Ltd, Stock-on-Trent, UK). The other starting chemicals were Na_2CO_3 (S/2880/60, Fisher Scientific, Leicestershire, UK), K_2CO_3 (P/4080/60, Fisher Scientific UK), $Mg(OH)_2$ (31 009-3, Aldrich Chemicals, Dorset, UK) and CaF_2 (23 794-9, Aldrich Chemicals). Batches were weighed out to two decimal places. Both compositions were melted in platinum-rhodium (2%) uncovered crucibles at 1400°C for 3 h in an electric furnace, and stirred for the final 2 h of the melt with a platinum stirrer (60 rpm). The melts were then cast as a block onto a steel plate. Glass samples were annealed by heating for 1 h at 550°–575°C, followed by cooling at 1°C/min to room temperature. Both glasses were clear after annealing, showing no devitrification or evidence of glass-glass phase separation. Heat treatment was performed isothermally, from 550°–1000°C for 4 h at 50° intervals and with heating and cooling rates of 5°C/min.

(2) Differential Thermal Analysis

Differential thermal analysis (DTA; Model DTA7, Perkin–Elmer Instruments, Norwalk, CT) was performed on −200 (<74 μm) mesh glass powders with a heating rate of 10°C/min to determine the glass-transition temperature (T_g) and onset temperature of crystallization (T_c). The reference sample for both compositions was α-alumina.

(3) X-Ray Diffraction (XRD)

For characterizing phases after heat treatment, an X-ray diffractometer (Philips, Eindhoven, Netherlands) with nickel-filtered Cu$K\alpha$ radiation operating at 30 mA and 50 kV was used. The scanning speed was set at 2° 2θ/min with a time per step of 0.02°. XRD was performed on −200 mesh (<74 μm) sieved powder samples.

(4) Transmission Electron Microscopy

Samples for transmission electron microscopy (TEM) were first mounted on a glass slide using a heat-sensitive resin and then ground to ~30 μm. A copper support ring was then glued to the sample using an epoxy resin. The sample was then removed from the slide and excess material chipped away from the support ring using a scalpel. For further thinning until perforation, a dual ion mill (Models 600 DP and 600 TMP, Gatan, Pleasanton, CA) was used at an angle of 11°–15°, a total beam current of 0.6 mA and at ~6 kV. Samples were carbon coated followed by examination using TEM (Model EM420, Philips) operating at 120 kV.

(5) Indentation Fracture Toughness

Samples (40 mm × 30 mm × 4 mm) were cut from the glass block using a precise diamond cut machine (Model Acutum 5, Struers, Copenhagen, Denmark) to create parallel faces. After heat treatment, they were ground and polished down to 1 μm using SiC paper and diamond paste. Indentations were made using a Vickers hardness testing machine (Vickers-Armstrong, Crayford, UK) for loads higher than 1 kg and a Vickers micro-hardness testing machine (Model M400, LECO Corp., St. Joseph, MO) for loads lower than 1 kg. For each load, at least 20–25 indentations were made and at least six (but often more than 15) readings were taken using an optical microscope (Vanox, Olympus Optical, Tokyo, Japan) equipped with a digital camera and computer (KS400 software, Imaging Associations, Thames, UK). Fracture toughness was calculated using the relations $K_c = 0.0824\ P/C^{3/2}$ (1) and $K_c = 0.0319\ P/a_o l^{1/2}$ (2) in the cases of median and Palmqvist cracks,[23] respectively, where K_c is indentation fracture toughness, P is the applied load, C is the crack size, a_o is Vickers indentation half-diagonal length, and $l = c - a_o$. The results are reported as mean values ± standard error. To evaluate the crack types (median/radial or Palmqvist) the samples were polished after indentation[24,25] and examined using either transmission or reflection optical microscopy. The as-cast glass exhibited indentations in which the cracks were of the median/radial type, but heat-treated samples showed either Palmqvist or median, dependent on temperature.

(6) Biaxial Flexural Strength

At least 10 disks (14 mm diameter and 3–5 mm thickness) for each series were core drilled from the as-cast glass plates and then ground to ~1 mm thickness. They were then heat-treated, ground, and polished down to 1 μm using SiC paper and diamond paste. A ball on ring test-jig was used for these samples attached to a

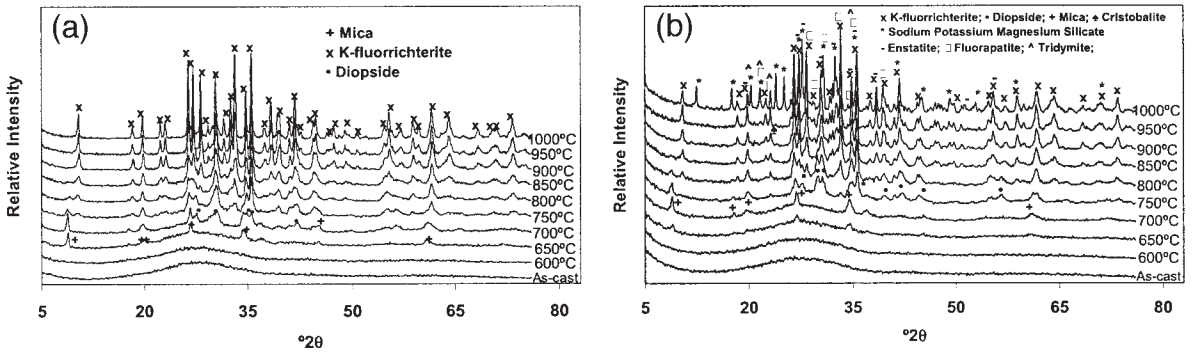

Fig. 2. XRD traces of (a) Glass A and (b) Glass B heat-treated at different temperatures.

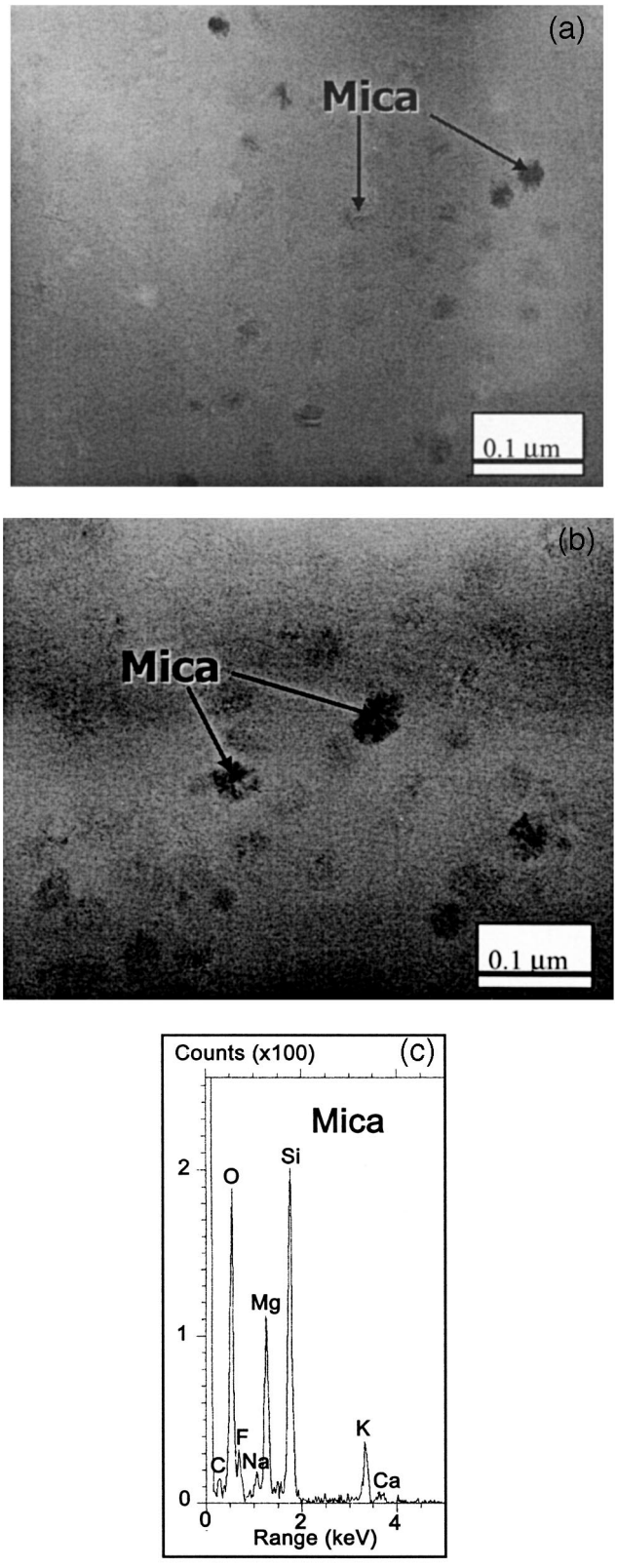

Fig. 3. Bright-field TEM images of (a) Glass A and (b) Glass B heat-treated at 650°C for 4 h along with (c) EDS trace of the small crystals shown in (a) and (b).

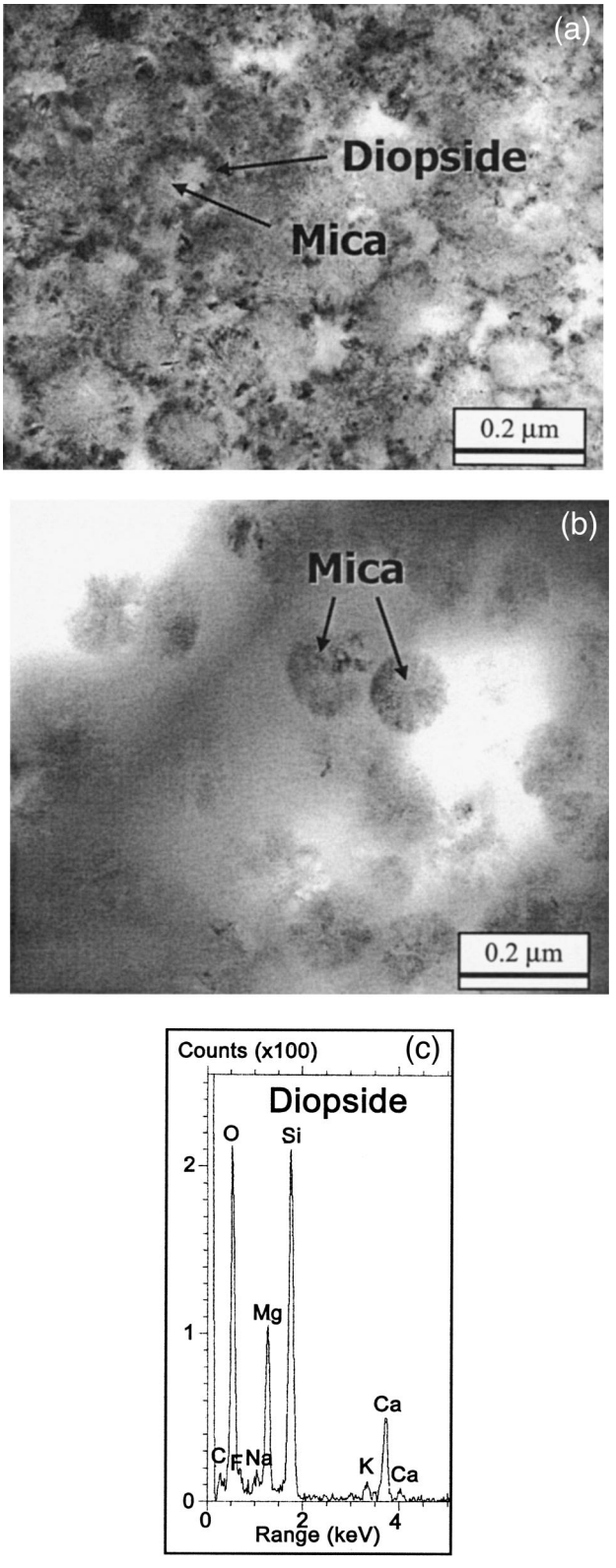

Fig. 4. Bright-field TEM image of (a) Glass A and (b) Glass B heat-treated at 700°C for 4 h along with (c) EDS trace of the dark regions (diopside) around the mica crystals shown in (a).

universal testing machine (Model 2000R, Lloyds Instruments, Fareham, Hampshire, UK) with a ring support of 9 mm at a cross-head speed of 1 mm/min. A piece of rubber sheet was positioned between the samples and support ring to remove any out of flatness and reduce friction as recommended in Ref. 26. The center of each disk was marked before testing to indicate the right position of the loading ball. The maximum stress, δ_{max}, at the center was calculated using the following equation:[27]

$$\sigma_{max} = \frac{3P(1+\nu)}{4\pi t^2}\left[1 + 2\ln\frac{r}{b} + \left(\frac{1-\nu}{1+\nu}\left\{1 - \frac{b^2}{2a^2}\right\}\frac{r^2}{R^2}\right)\right] \quad (1)$$

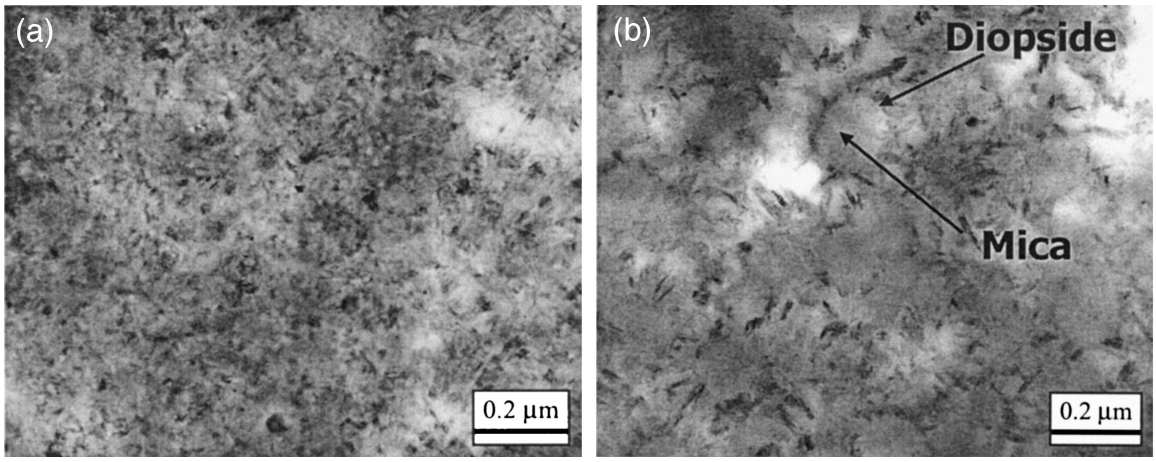

Fig. 5. Bright-field TEM image of (a) Glass A and (b) Glass B heat-treated at 750°C for 4 h.

where P is load, t is thickness, r is radius of the support ring, b is $t/3$, R is radius of the disk sample, and ν is Poisson's ratio. The final results are presented as mean values ± standard error.

III. Results and Discussion

(1) Phase Evolution

Figure 1 shows the DTA traces of glasses A and B. The glass transition temperatures (T_g) are 610°C and 597°C, respectively. The 13° difference may be attributed to the addition of P_2O_5 to Glass B, which weakens the silicate network and decreases the viscosity of the glass. In addition, both traces showed two large double exothermic peaks typical of crystallization events. The lower (in temperature) of the double peaks in each composition occurred at ~748°C, the second at 778°C and 832°C for Glass A and Glass B, respectively. Moreover, there was also a small anomaly at 922°C, in Glass B indicating a third crystallization event in this composition. Endothermic peaks corresponding to melting occurred at 1175°C and 1132°C in glasses A and B. In Glass A, however, the melting peak was narrower and deeper than in Glass B. This suggests that melting in Glass A may be congruent and associated largely with a single crystalline phase compared with Glass B, which has a wider peak, more typical of a multiphase sample exhibiting incongruent melting. Figures 2(a) and 2(b) are X-ray diffractograms that reveal the phase assemblage after isothermal heat treatment from 600°–1000°C for 4 h at 50°C intervals. Mica initially crystallized at 650°C in both Glass A and Glass B, followed by diopside at 700°C (Glass A) and 750°C (Glass B). At 750°C, there was evidence in each composition of peaks associated with K-fluorrichterite (KR), which increased in intensity up until 950°C. Furthermore, in Glass B, fluorapatite (FA) was present as a minor phase at >800°C. At >900°C in Glass A, KR was the sole crystalline phase, but in Glass B, KR, FA, cristobalite/trydimite, enstatite, and sodium potassium silicate phases were also present. The formation of the latter two phases in Glass B was accompanied by a decrease in the relative intensity of peaks associated with KR, in agreement with other researchers.[20] It is suggested that the formation of FA, $Ca_5(PO_4)_3F$, at 800°C in Glass B consumed calcium, fluorine along with phosphorus ions, which then disturbed the necessary oxide molar ratios for the formation of a single KR phase. The third exothermic peak in the DTA trace from Glass B may well be associated with the crystallization of either, cristobalite/trydimite, enstatite, or the sodium potassium silicate phase observed in samples heat-treated at 1000°C.

Figures 3(a) and 3(b) are TEM images showing the microstructure of Glass A and Glass B heat-treated 4 h at 650°C. EDS analyses (Fig. 3(c)) of the crystals shown in the two micrographs revealed that they are magnesium-rich and deficient in calcium with respect to the glass composition, consistent with the presence of mica ($KMg_{2.5}Si_4O_8F_2$) and in agreement with the XRD data (Fig. 2). Beall[9] suggested that glass in glass-phase separation occurs at ~550°C and that one of the glass phases is close to mica in composition. Although no direct evidence of phase separation is presented, the observations in both compositions were consistent with the concepts initially proposed by Beall[9] except more numerous and smaller mica crystals were observed in Glass A than Glass B, which contained P_2O_5. This shows that the nucleation rate of mica is lower in Glass B, however, its growth rate is higher, which can be attributed to the lower viscosity of the glass. The mechanism by which P_2O_5 decreased the nucleation rate of mica remains obscure, but it is possible that calcium and magnesium ions may associate with the PO_4^{3-} ions because of their high ionic field strength, increasing the tendency toward phase separation and inhibiting mica nucleation. A similar phenomenon has been reported in lithium disilicate system in which Li^+ associated with PO_4^{3-} ions and, in contrast, resulted in a higher volume fraction of crystalline silicate phase.[28]

Figures 4(a) and 4(b) are bright-field TEM images showing the microstructure of Glass A and Glass B after heat-treatment for 4 h at 700°C. In Glass A, a phase of darker contrast was present surrounding the mica crystals first observed in Fig. 3. This phase was magnesium deficient (Fig. 4(c)) compared with the mica crystals, consistent with the formation of diopside, as indicated in the XRD data (Fig. 2). In contrast, Glass B exhibited only crystals of mica, which were now larger than at 650°C. At 750°C (Fig. 5(a)), the microstructure was complex with individual crystals of mica, diopside, and KR, present according to XRD. These were difficult to resolve in projection through the sample because of their small size. In contrast, at 750°C in Glass B (Fig. 5(b)), a dark phase was observed around the mica crystals that was magnesium deficient, giving similar EDS traces to that shown in Fig. 4(c) and therefore consistent with the presence of diopside. The appearance of diopside at 750°C rather than at 700°C may explain the shift of 50°C upward in temperature for the second exothermic peak in the DTA trace from Glass B with respect to Glass A (Fig. 1). At 900°C, Fig. 6(a) revealed that Glass A contained a fine microstructure of lath-like crystals (<1 μm). XRD (Fig. 2) indicated that only KR was present in this composition, heat-treated at 900°C, which is known to have a lath-like morphology. A similar microstructure was observed for Glass B at 900°C (Fig. 6(b)), except that small equiaxed precipitates were also present, which EDS revealed (Fig. 6(c)) to contain only calcium and phosphorus cations. At 1000°C, Figs. 7(a) and 7(b), the microstructure of each composition coarsened considerably. Glass A (Fig. 7(a)) exhibited a bimodal distribution of crystal sizes (20 μm and 1 μm); however, XRD still indicated a single-phase KR composition. Moreover, EDS from the small and large crystals gave identical profiles, similar to the EDS trace for KR shown in Fig. 6(c). It was concluded, therefore, that both were K-fluorrichterite and that

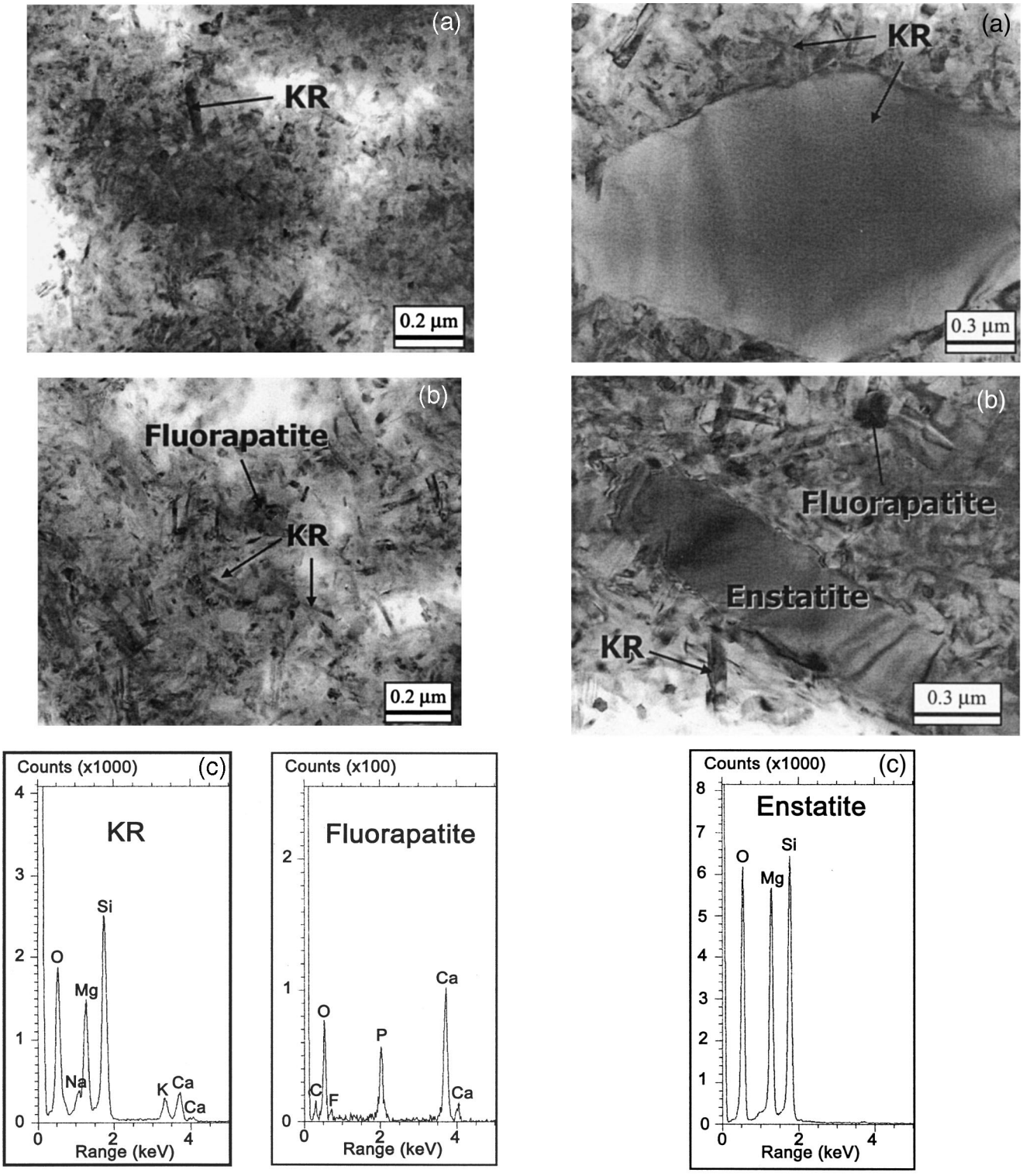

Fig. 6. Bright-field TEM image of (a) Glass A and (b) Glass B heat-treated at 900°C for 4 h along with (c) EDS traces of the matrix (K-fluorrichterite) phase shown in (a) and (b) and the equiaxed (fluorapatite) crystals shown by arrows in (b).

Fig. 7. Bright-field TEM image of (a) Glass A and (b) Glass B heat-treated at 1000°C for 4 h along with (c) EDS trace of the large (enstatite) crystal shown in (b).

abnormal crystal growth had occurred. The reason for the abnormal growth is unknown at this stage. In contrast, in Glass B heat-treated at 1000°C, the large crystals observed in Fig. 7(b) contained only magnesium and silicon cations consistent with the presence of enstatite, also identified in XRD traces (Fig. 2).

(2) Mechanical Properties

Figure 8 shows the indentation fracture toughness of Glass A and Glass B, as-cast and heat-treated at 900°, 950°, and 1000°C. The results showed an increase of fracture toughness from 0.7 ± 0.01 MPa·m$^{1/2}$ in the as-cast glass as temperature increases for both Glass A and Glass B. At <1000°C, the fracture toughness of Glass A and Glass B were within error identical. Surprisingly, however, there was large difference in fracture toughness between Glass A (1.59MPa·m$^{1/2}$) and Glass B (2.69 MPa·m$^{1/2}$) at 1000°C. The biaxial flexural strength (BFS) of polished samples is shown in Fig. 9. In Glass A, BFS values increased from 63.3 ± 4.5 MPa in the as-cast glass to the

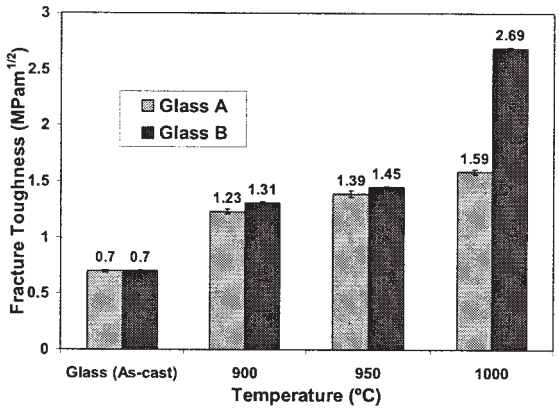

Fig. 8. Indentation fracture toughness of Glass A and Glass B heat-treated at different temperatures.

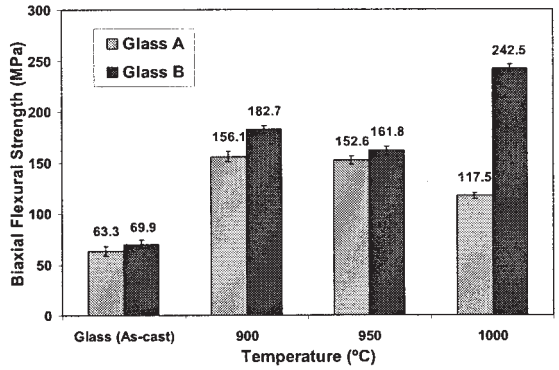

Fig. 9. Biaxial flexure strength of Glass A and Glass B heat-treated at different temperatures.

highest value of 156.1 ± 4.9 MPa at 900°C and then decreased to 117.5 ± 3.2 MPa at 1000°C. Similarly, in Glass B, BFS increased from 69.9 ± 4.2 MPa in the as-cast glass to 161.8 ± 4.4 MPa at 950°C; however, unlike Glass A, it rose to a maximum value of 242.5 ± 3.6 MPa at 1000°C.

For heat treatments ≤950°C, the fracture toughness of the glass compositions increased with temperature in a manner that may be explained by the formation of the highly interlocked fine-scale microstructure observed in the TEM (Figs. 5–7). However, at 1000°C, there was a marked increase in fracture toughness only for Glass B. Similarly, the BFS of Glass B was far in access of Glass A for samples heat-treated at 1000°C, even though at this temperature the microstructure had become multiphase rather than being composed solely of fine interlocked KR. This anomalous behavior, therefore, cannot be linked directly to the KR structure and microstructure. However, in Glass B heat-treated at 1000°C large lath-shaped enstatite crystals (Fig. 7(b)) with high aspect ratio (10:1) were present. Enstatite is thought to enhance fracture toughness owing to either residual stresses left because of the difference in thermal expansion coefficient between enstatite ($\sim 70 \times 10^{-7}°C^{-129}$) and the surrounding crystals, KR ($\sim 100 \times 10^{-7}°C^{-114}$), or more likely because of the presence of twin and cleavage planes in clino-enstatite crystals, which tend to deflect, branch, and blunt fractures.[9,29,30] Lee and Heuer[30] showed that even cooling of samples with 5°C/min was not slow enough to prevent proto-clino transformation and presence of twinned clino-enstatite was unavoidable. The presence of this strengthening phase in addition to FA and KR is ideal in a glass ceramic of this type. The main goal of the research was to develop a high-fracture toughness, castable glass ceramic biomaterial with osteoconductive properties. The *in vitro* and *in vivo* biological responses to KR-based compounds are currently being investigated. The presence of fluorapatite is associated with the osteoconductive property of bioceramics such as A/W glass ceramics, one of the few commercially successful glass-ceramic biomaterials. Therefore, P_2O_5-doped KR-based glasses show great promise as new bioceramics for bone tissue repair and augmentation.

V. Conclusions

(1) Stoichiometric K-fluorrichterite (Glass A) and stoichiometric with the addition of 2 mol% P_2O_5 (Glass B) both formed clear glass blocks on pouring.

(2) The phase evolution for this new glass ceramic (Glass B), as elucidated by XRD, was similar to that of Glass A (mica–diopside–K-fluorrichterite) except that fluorapatite was present at >800°C and enstatite at 1000°C.

(3) TEM images from Glass A and Glass B heat-treated at <950°C revealed a microstructure dominated by fine K-fluorrichterite crystals. However, at 1000°C, microstructure was coarser with large K-fluorrichterite (20 μm) and enstatite (10 μm) crystals observed in Glass A and Glass B, respectively.

(4) Heat-treatment of Glass B at 1000°C for 4 h results in a new glass ceramic with high-biaxial flexural strength (242.5 ± 3.6 MPa) and toughness (2.69 ± 0.01 $MPa \cdot m^{1/2}$), which contains KR as the main phase with minor phases of fluorapatite (a bioactive phase) and enstatite. The latter is thought to enhance fracture toughness and bend strength.

Acknowledgments

The authors are grateful to R. J. Hand for helpful discussions on mechanical properties. The authors would also like to thank P. Korgul, D. Bussey, and H. Bagshaw for their help with electron microscopy.

References

[1]W. Cao and L. L. Hench, "Bioactive Materials," *Ceram. Int.*, **22**, 493–507 (1996).
[2]C. A. Miller. I. M. Reaney, P. V. Hatton, and P.F. James, "Nucleation and Crystallisation of Canasite-Fluorapatite Glass Ceramics"; pp. 154–61 in *Proceedings of the International Symposium on Crystallisation in Glasses and Liquids*. Edited by W. Holand, M. Schweiger, and V. Rheinberger. Glasstech. Ber., Frankfurt, Germany, 2000.
[3]L. L. Hench, R.J. Splinter, W. C. Allen, and T. K. Greenlee, "Bonding Mechanism at the Interface of Ceramic Prosthetic Materials," *J. Biomed. Mater. Res.*, **2**, 117–41 (1972).
[4]T. Kokubo, S. Ito, S. Sakka, and T. Yammamuro, "Formation of a High-Strength Bioactiave Glass-Ceramic in the System MgO–CaO–SiO_2–P_2O_5," *J. Mater. Sci.*, **21**, 536–40 (1986).
[5]W. Vogel and W. Holand, "Development, Structure, Properties, and Application of Glass-Ceramics for Medicine," *J. Non-Cryst. Solids* **123**, 349–53 (1990).
[6]W. Holand, "Biocampatible and Bioactive Glass-Ceramics, State of the Art and New Directions," *J. Non-Cryst. Solids* **219**, 192–97 (1997).
[7]L. L. Hench, "Bioceramics," *J. Am. Ceram. Soc.*, **81** [7] 1705–28 (1998).
[8]T. Yamamuro, "A/W Glass-Ceramics: Clinical Applications"; pp. 89–103 in *An Introduction to Bioceramics*. Edited by L. L. Hench and J. Wilson. World Scientific, London, U.K., 1993.
[9]G. H. Beall, "Chain Silicate Glass-Ceramics," *J. Non-Cryst. Solids*, **129**, 163–73 (1991).
[10]V. M. da Rocha Barros, L. A. Salata, C. E. Sverzut, S P. Xavier, R. van Noort, A. Johnson, and P. V. Hatton, "*In Vivo* Bone Tissue Response to a Canasite Glass-Ceramic," *Biomaterials,* **23**, 2895–900, 2002.
[11]C. A. Miller, T. Kokubo, I. M. Reaney, P. V. Hatton, and P. F. James, "Formation of Apatite Layers on Modified Cansite Glass-Ceramics in Simulated Body Fluid," *J. Biomed. Mater. Res.*, **59**, 473–80 (2002).
[12]M. Cameron, S. Sueno, J. J. Papike, and C. T. Prewitt, "High Temperature Crystal Chemistry of K and Na Fluor-richterite," *Am. Mineral.* **68**, 924–43 (1983).
[13]A. Putnis, *Introduction to Mineral Science*. Cambridge University Press, Cambridge, U. K., 1993.
[14]G. H. Beall and J. E. Megles Jr., "Potassium Fluorrichterite Glass Ceramics and Method," U.S. Pat. No. 4 467 039, 1984.
[15]J. S. Huebner and J. J. Papike, "Synthesis and Crystal Chemistry of Sodium-Potassium Richterite $(Na,K)NaCaMg_5Si_8O_{22}(OH,F)_2$: A Model for Amphiboles," *Am. Mineral.*, **55**, 1973–92 (1970).
[16]D. G. Grossman, "Fluor-Amphibole Glass-Ceramics," U.S. Pat. No. 3 839 056, 1974.
[17]G. H. Beall, J. E. Mengles Jr., and L. R. Pinckney, "Glass-Ceramics Containing Cristobalite and Potassium Fluorrichterite," U.S. Pat. No. 4 608 348, 1986.
[18]A. A. Omar, A. W. A. El-Shennawi, and E. M. Hamzawi, "Effect of Isomorphous Substitutions on Crystallisation of Fluorrichterite Glasses," *Key Eng. Mater.*, **132–136**, 836–39 (1997).

[19]M. Mirsaneh, I. M. Reaney, and P. F. James, "Phase Evolution in K-Fluorrichterite Glass-Ceramics," *Phys. Chem. Glasses,* **43C,** 317–20 (2002).

[20]A. W. A. El-Shennawi, A. A. Omar, and E. M. A. Hamzawy, "Role of Fluorine and Phosphorus in the Crystallisation of K-Richterite Glass"; in *Proceedings of the 18th International Congress on Glass.* Edited by M. K. Choudhary, N. T. Huff, C. H. Drummond. American Ceramic Society, Westerville, OH, 1998.

[21]I. L. Denry and J. A. Holloway, "Effect of Magnesium Content on the Microstructure and Crystalline Phases of Fluoramphibole Glass-Ceramics," *J. Biomed. Mater. Res*, **53**, 289–96 (2000).

[22]I. L. Denry and J. A. Holloway, "Effect of Sodium Content on the Crystallisation Behaviour of Fluoramphibole Glass-Ceramics," *J. Biomed. Mater. Res.*, **63**, 48–52 (2002).

[23]C. B. Ponton and R. D. Rawlings, "Vickers Indentation Fracture Toughness Test: Part 1, Review of Literature and Formation of Standardised Indentation Toughness Equations," *Mater. Sci. Technol.*, **5**, 865–72 (1989).

[24]C. B. Ponton and R. D. Rawlinlgs, "Vickers Indentation Fracture Toughness Test: Part 2, Application and Critical Evaluation of Standardized Indentation Toughness Equations," *Mat. Sci. Technol.*, **5**, 961–76 (1989).

[25]R. L. K. Matsumoto, "Evaluation of Fracture Toughness Determination Methods as Applied to Ceria-Stabilized Tetragonal Zirconia Polycrystal," *J. Am. Ceram. Soc.,* **70** [12] C366–C368 (1987).

[26]R. Morrell, *Biaxial Flexural Strength Testing of Ceramic Materials*, National Physical Laboratory, Teddington, Middlesex, U.K., 1998.

[27]D. K. Shetty, R. D. Rosenfield, P. McGuire, G. K. Bansal, and W. H. Duckworth, "Biaxial Flexure Tests for Ceramics," *Bull. Am. Ceram. Soc.,* **59** [12] 1193–97 (1980).

[28]P. F. James and P. W. McMillan, "Quantitative Measurements of Phase Separation in Glasses Using Transmission Electron Microscopy: Part 2, A Study of Lithia-Silica Glasses and the Influence of Phosphorus Pentaoxide," *Phys. Chem. Glasses*, **11** [3] 64–70 (1970).

[29]G. H. Beall, "Refractory Glass-Ceramics Containing Enstatite," U.S. Pat. No. 4 687 749, 1987.

[30]W. E. Lee and A. H. Heuer, "On the Polymorphism of Enstatite," *J. Am. Ceram. Soc.* **70** [5] 349–360 (1987). □